Ultra-fast Laser Processing

Mater. Res. Soc. Symp. Proc. Vol. 1365 © 2011 Materials Research Society
DOI: 10.1557/opl.2011.1220

Transient Localized Material Properties Changes by Ultrafast Laser-Pulse Manipulation of Electron Dynamics in Micro/Nano Manufacturing

Xin Li[1], Lan Jiang[1*], Cong Wang[1] and Hai-Lung Tsai[2]
[1]Laser Micro/Nano Fabrication Laboratory, School of Mechanical Engineering, Beijing Institute of Technology, Beijing 100081, People's Republic of China
[2]Laser-Based Manufacturing Laboratory, Department of Mechanical and Aerospace Engineering Missouri University of Science and Technology, Rolla, MO 65409, USA

ABSTRACT

A femtosecond (fs) pulse duration is shorter than many physical/chemical characteristic times, such as the electron-photon relaxation time, which makes it possible to control electron dynamics. This paper reviews our recent progress which proposes to change electron dynamics (selective excitation/ionization) and electron densities/temperatures in materials to control the following properties and processes: 1) the transient (femtosecond-to-picosecond time scale), localized (nanometer-to-micrometer length scale) material properties, 2) the corresponding photon absorption process, and 3) phase change mechanisms, by manipulating fs pulse-train number/delay for high-precision micro/nanoscale manufacturing.

INTRODUCTION

Femtosecond (fs) lasers, with short pulse duration compared with many physical/chemical characteristic times and extremely high irradiance, lead to a new area of ultrafast science and technology, which introduce new phenomena, requiring new experimental and theoretical understanding [1-3]. Recently, developments of optics devices have made fs pulse-train design possible by shaping classic Gauss shape fs pulses to arbitrary shape fs pulses [4], which offer us great opportunity for controlling electron dynamics [5-7]. In this paper, our recent progress is reviewed on the studies of changing electron dynamics to control the following properties and processes by fs pulse-train design for high-precision micro/nanoscale manufacturing [8, 9].

THEORY

For dielectrics, the first-principles calculation (time-dependent density-functional theory, TDDFT) is adopted to study the electron dynamics (selective excitation/ionization) by fs pulse-train irradiation. The time-dependent Kohn-Sham (TDKS) equation for single particle orbitals is applied to describe the motion of electrons [10].

$$i\hbar\frac{\partial}{\partial t}\psi_i(\vec{r},t) = H_{KS}(\vec{r},t)\psi_i(\vec{r},t) \qquad (1)$$

* Author to whom correspondence should be addressed. Electronic address: jianglan@bit.edu.cn.

$$n(\vec{r},t) = \sum_i \left|\psi_i(\vec{r},t)\right|^2 \quad (2)$$

where $n(\vec{r},t)$ is the electron density, $H_{KS}(\vec{r},t)$ is the Kohn-Sham Hamiltonian which is conventional separated in the following way,

$$H_{KS}(\vec{r},t) = \frac{1}{2m}(\vec{p} + \frac{e}{c}\vec{A}(t))^2 + V_{ion}(\vec{r},t) + e^2\int d\vec{r}'\frac{n(\vec{r},t)}{\left|\vec{r}-\vec{r}'\right|} + V_{xc}(\vec{r},t) \quad (3)$$

where e is an elementary charge, $\vec{A}(t)$ is a time-dependent spatially-uniform vector potential which is related to the external electric field, $V_{ion}(\vec{r},t)$ is the electron-ion potential and $V_{xc}(\vec{r},t)$ is the exchange-correlation potential.

For metals, a model combined two-temperature model and molecular dynamics simulation is adopted to explore the phase change mechanisms by fs pulse-train design [9]. The two temperature model treats electrons and lattices as two separate subsystems

$$C_e(T_e)\frac{\partial T_e}{\partial t} = \nabla\left[k_e(T_e)\nabla T_e\right] - G(T_e - T_l) + S(z,t)$$
$$C_l(T_l)\frac{\partial T_l}{\partial t} = G(T_e - T_l) \quad (4)$$

where T_e is electron temperature, T_l is lattice temperature, C_e is electron heat capacity, C_l is lattice heat capacity, k_e is electron heat conductivity, G is electron-lattice coupling factor. And the Morse potential is used for interactions among nickel atoms.

$$\Phi(r_{ij}) = D\left(e^{-2\alpha(r_{ij}-r_0)} - 2e^{-\alpha(r_{ij}-r_0)}\right) \quad (5)$$

where $\Phi(r_{ij})$ is the potential energy of two atoms i and j separated by a distance r_{ij}.

DISCUSSION

Fs pulse-train ablation of dielectrics

In first-principles calculation, an orthorhombic unit cell of SiO_2 is modeled with lattice constants of 9.29*a.u.*, 16.09*a.u.* and 10.21*a.u.* along x, y and z axis respectively. Calculations are based on density functional theory (DFT) within the adiabatic local density approximation. The laser irradiation is modeled by subjecting the system to an external alternating electric field parallel to z axis. In addition, the ion position is frozen in all the calculations.

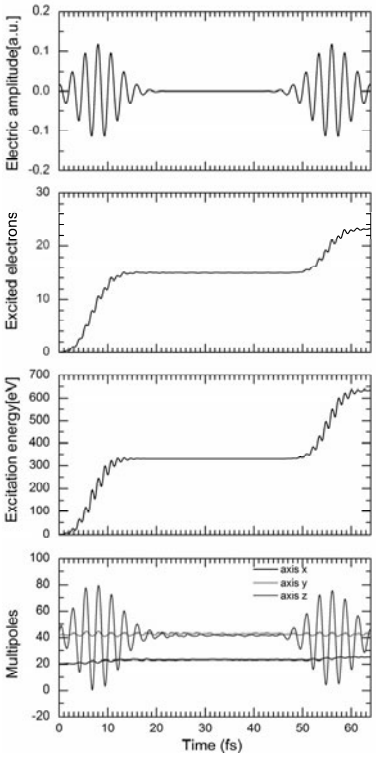

Figure 1. Laser electric field, excited electrons, excitation energy and multipoles.

Figure 1 shows the electron dynamics by fs pulse-train ablation of dielectrics, where the fs pulse-train consists of two sub-pulses with a separation time of 48 fs. Each of sub-pulse is a Gaussian wave packet with wavelength of 800nm, pulse duration of 16fs, peak power density of 5×10^{14} W/cm^2, as shown in figure 1a. Figure 1b shows that the number of excited electrons with time. At the initial stage, as laser electric field is weak, only a small amount of electrons are excited. However, an abrupt change occurs after 4fs, which is considered as a sign of the optical breakdown. Then the number of excited electrons reaches a first saturation value at around 12 fs during the first sub-pulse and a second saturation value at around 56 fs during the second sub-pulse. Figure 1c shows that the excitation energy or the total energy absorbed from laser electric field exhibits the similar evolution rules as the number of excited electrons. After laser irradiance, the total absorbed energy is 635.5eV and the average energy per excited electron is 27.38eV. Figures 1d shows that multipoles along z axis exhibit a 1-2 fs delay following laser electric field, whereas multipoles along x,y axis exhibit only slight disturbance. And multipoles reach the

amplitude at around 8 fs and 56 fs with a smaller value of the second sub-pulse, which is due to the impact of a potential induced by free electron generations that weakens laser electric field.

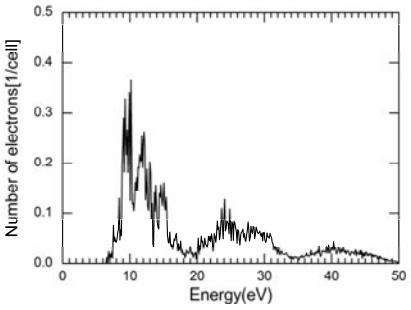

Figure 2. Occupation of excited electrons in the conduction band after laser irradiance.

Figure 2 shows the occupation of excited electrons in the conduction band after laser irradiance. As the laser power density (5×10^{14} W/cm^2 for each sub-pulse) is high enough for fully ionization of materials, the excited electrons are distributed broadly between 7-50eV.

Fs pulse-train ablation of metals

In the model combined two-temperature model and molecular dynamics simulation, nickel thin films are 18nm×2nm×200nm with periodic boundary conditions along x,y axis and free boundary conditions along z axis. Fs pulse-train design is employed by shaping single Gauss pulses to pulse-trains consisting of sub-pulses with different number/delay, as shown in figure 3.

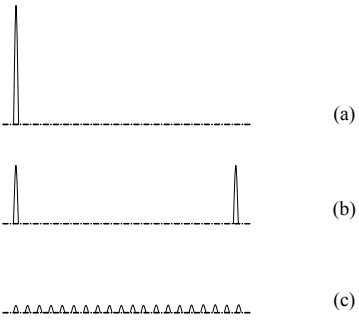

Figure 3. Schemes of fs pulse-train with the same total laser fluence. (a) classic fs pulse, (b) pulse-train with 2 sub-pulses with a separation time of 20 fs, (c) pulse-train with 20 sub-pulses with a separation time of 1 fs.

Figure 4 shows the snapshots of nickel thin films irradiated by fs pulse-train with the total laser fluence of 0.28J/cm^2, which indicates that fs pulse-train design dramatically changes electron dynamics and following energy transport and phase change processes [9]. For single pulse case, the nickel film fractures from inside accompanying several gas bubbles generation. For pulse-train with 2 sub-pulses case, the film fracture is weakened. For pulse-train with 20 sub-pulses case, the nickel film decomposes from the uppermost film without gas bubbles generation, which also leads to lower ablation rate with more and smaller uniform nanoparticles.

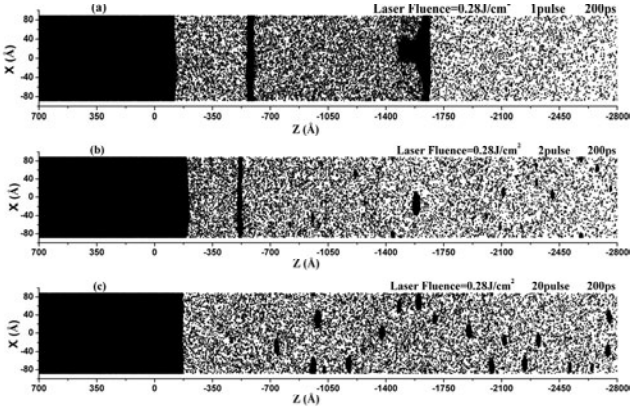

Figure 4. The snapshots of nickel thin films irradiated by fs pulse-train with the total laser fluence of 0.28J/cm^2. (a) classic fs pulse, (b) pulse-train with 2 sub-pulses with a separation time of 20 fs, (c) pulse-train with 20 sub-pulses with a separation time of 1 fs [9].

Figure 5 shows the time evolution of the dynamic film surfaces in ρ-T plane. For single pulse case, materials get across binodal line and approach spinodal line, where phase explosion is dominant mechanism. For pulse-train with 2 sub-pulses case, laser energy is inclined to deposit within film surface, and materials can get across both binodal and spinodal line. Still, phase explosion is dominant mechanism. For pulse-train with 20 sub-pulses case, materials can be heated to extremely high temperature and directly achieve supercritical state, where critical point phase separation is dominant mechanism.

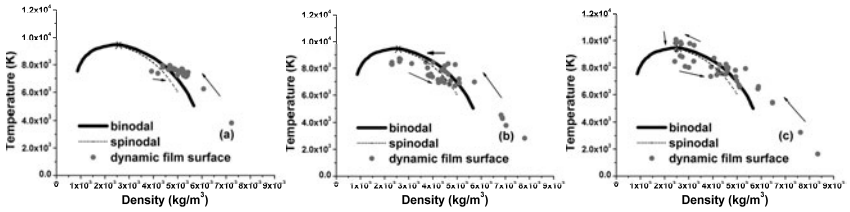

Figure 5. Time evolution of the dynamic film surfaces in ρ-T plane. (a) classic fs pulse, (b) pulse-train with 2 sub-pulses, (c) pulse-train with 20 sub-pulses [9]

CONCLUSIONS

This paper reviews our recent progress on the studies of changing electron dynamics to control the following properties and processes by fs pulse-train design for high-precision micro/nanoscale manufacturing. For dielectrics, first-principles calculation validates the feasibility of controlling electron dynamics by fs pulse-train irradiation. For metals, combined model predicts the electron dynamics and following energy transport and phase change processes can be dramatically changed by fs pulse-train design, which may favor high-precision micro/nanoscale manufacturing.

ACKNOWLEDGMENTS

This work was supported by the National Natural Science Foundation of China (NSFC) (Grants No. 90923039 and 51025521) and the 111 Project of China (Grant No. B08043).

REFERENCES

1. Y. Y. Cao, N. Takeyasu, T. Tanaka, X. M. Duan, and S. Kawata, *Small* 5, 1144 (2009).
2. A. Y. Vorobyev, and C. Guo,ion, *Phys. Rev. B* 72,195422 (2007).
3. Z. Hu, S. Singha, and R. J. Gordon, *Phys. Rev. B* 82, 115204 (2010).
4. L. Jiang, and H. L. Tsai, *Appl. Phys. Lett.* 87, 151104 (2005)
5. M. Spyridaki, E. Koudoumas, P. Tzanetakis, C. Fotakis, R. Stoian, A. Rosenfeld, and I. V. Hertel, *Appl. Phys. Lett.* 83, 1474 (2003).
6. R. Hergenröder, M. Miclea, and V. Hommes, *Nanotechnology* 17, 4065 (2006).
7. S. Noël and J. Hermann, *Appl. Phys. Lett.* 94, 053120 (2009).
8. L. Jiang, and H. L. Tsai, *Int. J. Heat Mass Transfer* 48, 487 (2005)
9. X. Li, L. Jiang, and H. L. Tsai, *J. Appl. Phys.* 106, 064906 (2009).
10. M. A. L. Marques, E. K. U. Gross, *Annu. Rev. Phys. Chem.* 55, 427 (2004).

Mater. Res. Soc. Symp. Proc. Vol. 1365 © 2011 Materials Research Society
DOI: 10.1557/opl.2011.1036

Nanomorphing with Ultrafast Lasers and Biomedical Applications

Alan J. Hunt
Department of Biomedical Engineering
University of Michigan,
Ann Arbor, MI, 48109 U.S.A.

ABSTRACT

Classically, the limit for optical machining is on the order of the wavelength of the incident light. However, by taking advantage of precise, nonlinear damage mechanisms that occur for femtosecond laser pulses, damage can be achieved on a scale an order of magnitude lower, allowing precise removal of very small amounts of material to produce holes mere tens of nanometers wide. Femtosecond laser nanomachining can be carried out in a variety of dielectrics, and in transparent substrates machining can be sub-surface, in contrast to other nanomachining techniques such as using an electron beam or focused ion beam. We focus on the use of glass, as it is in many ways an ideal material for use in biological applications due to its chemical, optical, electrical and mechanical properties. By precisely placing laser pulses in glass, three dimensional nano and microfluidic channels and devices can be formed including nozzles, mixers, and separation columns. Recent advances in this technique allow the formation of high aspect ratio nanochannels from single pulses, thus helping address the fabrication speed limitations presented by serial processing. These nanochannels have a range of applications including the fabrication of nanoscale pores and nanowells that may serve as vias between fluidic channels, or from channels to a surface. These nanochannels have applications as a standalone technique for fabrication of nanopores and nanowells, but can also complement other fabrication techniques by allowing precisely placed jumpers that can connect channels that are out of plane. We discuss applications for diagnostic microfluidic devices, and basic cell biology research.

INTRODUCTION

The macromolecular machinery that supports cellular functioning principally operates on the scale of nanometers, and nanoscale science and technology are broadly recognized as important emerging disciplines with broad potential to impact the development of new drugs and diagnostic devices. A principal challenge to realizing this potential is the difficulty of precise modification of materials at the micro and nanometer scales. This can be addressed by femtosecond laser nanomachining and ablation. Damage produced by femtosecond (fs) laser pulses is extraordinarily precise when the energy is near the damage threshold, that is at "critical intensity" (Joglekar et al., 2004). Indeed the precision of optics at critical intensity is so great that it enables laser machining of features that are far smaller than the limits that diffraction typically places on optical techniques (Du et al., 1996; Joglekar et al., 2003; Joglekar et al., 2004; Pronko et al., 1995; Temnov, 2006; Venkatakrishnan et al., 2002), and we have demonstrated precision down to the nanoscale (Joglekar et al., 2003; Joglekar et al., 2004), producing features as small as 20 nm in dielectrics. Nanometer scale features can also be fabricated in heterogeneous materials, including biological materials. Thus femtosecond nanomachining can

produce features at a scale that competes with e-beam or ion-beam lithography, but is relatively simple to execute as it does not require a vacuum or special materials. Additionally, due to the sharp spatial confinement of femtosecond laser damage, chemical and structural changes are minimal beyond the ablated region. Furthermore, since this is an optical technique, it uniquely allows subsurface modification in optically transparent materials. By enabling such precise 3D fabrication or ablation, optical nanomachining constitutes a powerful tool for selectively ablating biological structures, and machining components for novel diagnostic and research devices.

EXPERIMENT

Here we present an overview of applications of femotosecond laser nanomachining and ablation that are being developed in our group. The following topics will be discussed:

1) Chemical separation. We have developed strategies to optimize debris clearing by expanding microbubbles produced during machining in liquids (Ke, 2005; Lee, 2007). This enables fabrication of long, thin (~0.5 micron) channels with aspect ratios greater than 1000:1. We have applied this to create an exceptionally small nanoscale capillary electrophoresis device that can perform a chemical separation using femtoliter sample volumes in under one second. Substances to be analyzed are introduced into the loading column by electroosmotic flow, and a fluid plug is pulled into the spiral separation column by switching the potential from

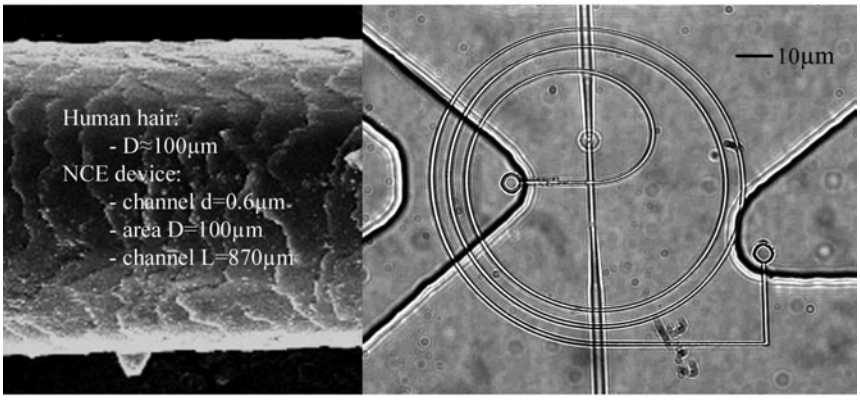

Figure 1. A functional nanoscale capillary electrophoresis device (right) compared with a hair (left). Vertical structure is a loading column, spiral is the separation column. Larger structures on right and left are the overlying PDMS header.

across the loading channel to across the separation column. As the analyte moves through the spiral, differential partitioning between fluid and solid phases (i.e. binding and unbinding to the channel walls) results in separation of substances as the fluid proceeds through the column.

2) Sensors and chemical analysis. The high-precision and repeatability of femtosecond laser damage allows machining of conical pores in glass, and these can be applied to detect